



# Superficial visible-light-responsive Pt@ZnO nanorods photocatalysts for effective remediation of ciprofloxacin in water

Nadiyah Alahmadi • M. S. Amin • R. M. Mohamed

Received: 17 June 2020 / Accepted: 29 July 2020 / Published online: 1 August 2020  
© Springer Nature B.V. 2020

**Abstract** Fabrication of mesoporous ZnO nanorods photocatalysts exploiting a facile one-pot regime of zinc methoxide and F127 triblock copolymer as a surfactant was conducted. The impact of decoration with platinum on the photocatalytic efficacy, crystallinity, morphology, and physical aspects of mesoporous Pt@ZnO nanorods accommodating various proportions of Pt was interrogated. TEM micrographs affirmed that the fabricated mesoporous ZnO nanorods displayed nanorods architecture and platinum was doped on the surface of mesoporous ZnO nanorods as dots. The measured lattice spacing of the (002) plane of ZnO was found to be about 0.270 nm, affirming the development of the ZnO lattice architecture. On the other hand, the consistent lattice spacing of the (111) plane of Pt was 0.220 nm, endorsing the progression of the metallic platinum lattice architecture. Evidently, the surface area possessed

by the fabricated mesoporous ZnO nanorods was 200 m<sup>2</sup>/g; up to our knowledge, this large surface area wasn't attained previously. Furthermore, the average pore diameter and the total pore volume possessed by the fabricated mesoporous ZnO nanorods photocatalyst were 6.90 nm and 0.140 cm<sup>3</sup>/g, respectively. Ciprofloxacin (CIP) was photocatalytically degraded adopting mesoporous ZnO nanorods photocatalyst with a performance of 10%, whereas the photocatalytic performance toward CIP destruction was enhanced up to 100% upon doping ZnO nanorods photocatalyst with 0.6 wt.% Pt. Also, doping of the mesoporous ZnO nanorods photocatalyst with 0.6 wt.% Pt enhanced the photocatalytic degradation rate by 14 times compared with that of mesoporous ZnO nanorods photocatalyst. This conclusion could be attributed to the development of a high concentration of hydroxyl radicals, the accelerated

---

This article is part of the topical collection on *Nanotechnology in Arab Countries*

---

Guest Editor: Sherif El-Eskandarany

---

N. Alahmadi  
University of Jeddah, College of Science, Department of  
Chemistry, Jeddah, Saudi Arabia

M. S. Amin  
Chemistry Department, Faculty of Science, Ain Shams University,  
Abbassia, Cairo, Egypt

M. S. Amin  
Chemistry Department, College of Science, Taibah University,  
Al-Madinah Al-Munawarah, Saudi Arabia

R. M. Mohamed  
Department of Chemistry, Faculty of Science, King Abdulaziz  
University, P.O. Box 80203, Jeddah 21589, Kingdom of Saudi  
Arabia

R. M. Mohamed (✉)  
Advanced Materials Department, Central Metallurgical R&D  
Institute, CMRDI, P.O. Box 87, Helwan, Cairo 11421, Egypt  
e-mail: redama123@yahoo.com

dissipation of ciprofloxacin molecules to the active centers of the developed photocatalyst in addition to the reduced light scattering owing to the large surface area and high pore volume of the photocatalyst.

**Keywords** Triblock copolymer · Mesoporous ZnO · Nanorods · Photocatalytic performance · Environmental and health effects

## Introduction

It is well-known that CIP, a fluoroquinolone antibiotic, could dissipate easily to the environment owing to its weak degradation via metabolism beyond utilization by humans. Numerous investigations affirmed the detection of CIP with pronounced quantities in the environment (Antonin et al. 2015; An et al. 2010). Diverse methods have been developed for degradation of CIP like membrane (Elhalil et al. 2016), Fenton (Sacco et al. 2018), adsorption (Mahjoubi et al. 2016), biological (Bonakdarpour et al. 2011), and coagulation/flocculation (Freitas et al. 2015) treatments. Nevertheless, the trials to get rid of CIP via these conventional regimens from wastewater were not effective for complete degradation (Taheran et al. 2016; Daughton and Ternes 1999; Bolong et al. 2009; Chakraborty et al. 2017). Accordingly, many attempts have emerged for pharmaceutical pollutants remediation from wastewater via adequate, efficient, and eco-friendly regimes. Owing to its great efficacy, photocatalysis has been emerged as one of the most adequate regimes to remediate CIP from the aquatic environment (Li et al. 2003; Ravelli et al. 2009; Yuan et al. 2016; Mohamed et al. 2017; Mohamed 2009; Mohamed and Aazam 2013; Mohamed et al. 2012; Mohamed and Salam 2014; Ismail et al. 2006). Furthermore, photocatalyses are distinct by their capability to remove very low doses of pollutants from the aquatic environment in an efficient manner (Abdennouri et al. 2015). Photocatalytic processes could be accomplished by adopting numerous semiconductors (Sohabi et al. 2017; Sobahi et al. 2018; Baoum et al. 2018; Baoum et al. 2020; Sobahi and Amin 2020). Owing to its efficient and powerful photocatalytic features, zinc oxide (ZnO) has been emerged to the area of photocatalysis as an adequate semiconductor (Vaiano et al. 2017; Ullah and Dutta 2008; Suryavanshi et al. 2018) in comparison with TiO<sub>2</sub> (Daneshvar et al. 2004; Kansal et al. 2007; Hariharan 2006). The most important advantage that characterizes ZnO is its capability to absorb a greater fraction of solar

spectra compared with that of titania (Miyauchi et al. 2002). Nevertheless, ZnO possesses a large band gap value (3.3 eV) and so it displays fast reconsolidation amid the photo-generated charge carriers (Djurišić and Leung 2006). Accordingly, ZnO displays hindered photocatalytic performance owing to the inefficient utilization of sunlight (Sardar et al. 2017). It is well-known that the Vis light fraction of the solar spectrum is about 40% and so, the attempts of scientists are concerned with customization of the ZnO catalyst to be applied beneath Vis light (Wang et al. 2013; Kochuveedu et al. 2013). Many attempts have been achieved to improve the application of ZnO catalyst beneath Vis light through diminishing the reconsolidation amid the photo-generated charge carriers like metal deposition (Vaiano et al. 2018; Jaramillo-Páez et al. 2018; Liqiang et al. 2006), hybridization with carbon materials (Mu et al. 2011), combination with another semiconductor (Yu et al. 2013; Ma et al. 2014), and decoration with metal or non-metal elements (Vaiano et al. 2017; Qiu et al. 2008; Sudrajat and Babel 2017; Bousslama et al. 2017). One of the successful regimes to extend the life time of the generated charge carriers without combination (Sardar et al. 2017) is the noble metal deposition on the photocatalyst which may be adopted via deposition of Au (Sarkar et al. 2011; Pirhashemi et al. 2018; Shekofteh-Gohari et al. 2018), Pt (Shekofteh-Gohari et al. 2018; Akhundi et al. 2019), Ag (Sudrajat and Babel 2017; Vijayan et al. 2020; Wang et al. 2016; Wang et al. 2015; Georgekutty et al. 2008), and Pd (Wang et al. 1992). Furthermore, one of the advantages that characterize noble metals is their great capability to absorb light spectrum in the Vis light zone owing to the presence of surface plasmon resonance (Truong et al. 2013). Hence, deposition of noble metal on ZnO semiconductor encourages the later to be applied beneath Vis light region. In this situation, the adopted semiconductors are acknowledged as plasmonic photocatalysts (Tanaka and Kominami 2016; Wang et al. 2012). Evidently, excited electrons possess sufficient energy that makes them able to transfer to the conduction band (CB) of the photocatalyst. Numerous investigations were performed on the improvement of photocatalytic efficacy of titania or ZnO via noble metal deposition (Liu et al. 2018; Cai et al. 2018; Zhang et al. 2016; Lin et al. 2009). Furthermore, remediation of some pollutants was investigated adopting the upgraded titania after noble metal deposition (Plodinec et al. 2014; Jodat and Jodat 2014).

Up to our knowledge, there are insufficient examinations about photocatalytic destruction of pharmaceutical compounds beneath Vis light illumination adopting

upgraded ZnO after modification with diverse noble metals. Our work aims to examine the photocatalytic destruction of CIP beneath Vis light irradiation adopting upgraded ZnO after Pt deposition. Photocatalytic performance of 0, 0.2, 0.4, 0.6, and 0.8 wt.% Pt@ZnO nanorods photocatalysts was evaluated beneath Vis light illumination. Besides, the effect of the fabricated nanorods photocatalysts dosage on the photocatalytic performance toward CIP destruction was also examined.

## Experimental

### Chemicals and reagents

All chemicals and reagents in this inspection were appropriated without any treatment as acquired from Sigma-Aldrich. The adopted chemicals were  $\text{H}_2\text{PtCl}_6 \cdot 6\text{H}_2\text{O}$  and Zinc methoxide, whereas absolute ethyl alcohol, acetic acid ( $\text{CH}_3\text{COOH}$ ), and hydrochloric acid (HCl) were handled as reagents. On the other hand, the F-127 surfactant was appropriated as a block copolymer.

### Fabrication of mesoporous ZnO nanorods photocatalyst

F-127 surfactant was endorsed as a template to fabricate mesoporous ZnO nanorods photocatalyst supporting a facile regime. ZnO, F-127 surfactant, ethyl alcohol, hydrochloric acid, and acetic acid were appropriated with the molar ratio of 1: 0.02: 50: 2.25: 3.75. Typically, F-127 surfactant (1.6 g) was combined to 30 mL of absolute ethyl alcohol and the mixture was agitated magnetically for 1 h. After that, 3.5, 2.3, and 0.74 mL of Zinc methoxide,  $\text{CH}_3\text{COOH}$ , and HCl, respectively, were introduced to the previous mixture. The attained mixture was left to dry for 12 h in a relative humidity of 50–70% and a temperature of 40 °C to activate the polymerization of both F-127 surfactant and zinc ions. The resultant sample was left to dry for 12 h at a temperature of 65 °C. The ultimate yield was fired for 4 h at 450 °C to attain mesoporous ZnO nanorods (ZNO) photocatalyst.

### Fabrication of Pt@ZnO nanorods photocatalysts

Deionized water (100 mL) was appropriated to disperse the previously fabricated ZNO (100 mg). By dissolving computed quantities of  $\text{H}_2\text{PtCl}_6 \cdot 6\text{H}_2\text{O}$  in the prior dispersion, 0.2, 0.4, 0.6, and 0.8 wt.% Pt@ZnO nanorods

photocatalysts were attained. After that, the Xe arc lamp (500 W) was applied for 1 day to irradiate the formerly realized mixture. The product was then washed with deionized water and ethanol three times, and subsequently, it was centrifuged at 10000 rpm. The attained powder was heated for 2 h at 100 °C. The accessed specimens were designated as 0.2 Pt@ZNO, 0.4 Pt@ZNO, 0.6 Pt@ZNO, and 0.8 Pt@ZNO.

### Identification of the fabricated nanorods photocatalysts

Diverse tools were exploited to identify the fabricated nanorods photocatalysts. X-ray diffraction (XRD) investigation was achieved to inspect phase architecture of the developed photocatalysts accommodating diverse proportions of Pt. It was performed via the utilization of Cu K $\alpha$  radiation ( $\lambda = 0.154$  nm), whereas Thermo Scientific spectrometer (K-ALPHA) was endorsed to present the X-ray photoelectron spectroscopy (XPS) evaluations. Microstructure and morphology of the fabricated nanospecimens were explored via covering a transmission electron microscope (TEM) of JEOL kind. Chromatech device of Nova series was appropriated to achieve adsorption-desorption isotherms at 77 K using nitrogen gas. Such analysis was adopted to attain surface area and surface texture of the fabricated nanorods. Before adsorption experiments, specimens were outgassed for 2 h at 100 °C in a vacuum. On the other hand, the UV-VIS-NIR spectrophotometer of the Jasco model was appropriated to inspect the light absorption spectra. UV-Vis diffuse reflectance spectra (DRS) were adopted to evaluate binding energy ( $E_g$ ) for all fabricated nanorods photocatalysts. Furthermore, photoluminescence emission spectra (PL) of the fabricated nanorods photocatalysts were deliberated via covering the fluorescence spectrophotometer of the Shimadzu model. Finally, electrochemical workstation (Zahner Zennium) was administered to appraise photocurrent intensity of the fabricated nanorods photocatalysts.

### Photocatalytic performance examination

Vis light ( $\lambda > 420$  nm) illumination was practiced to estimate the photocatalytic destruction of 10 ppm ciprofloxacin (CIP) in aquatic solution over the fabricated Pt@ZnO nanorods photocatalysts accommodating diverse proportions of Pt metal. To attain only spectra with  $\lambda > 420$  nm, a cut-off filter was exploited to eradicate spectra of  $\lambda < 420$  nm. Xenon lamp (300 W) was practiced on the upper part of the reactor containing the

reaction mixture to accomplish the photocatalytic degradation process. The lamp was afforded with a cooling tube via water circulation to avoid heating. Photocatalytic degradation reaction was implemented in a 50-mL special quartz reactor. Evidently, the computed quantity of the fabricated nanorods photocatalyst was suspended in the photo-reactor to inspect the photocatalytic destruction of the pharmaceutical compound (CIP). Air was pumped to the suspension solution throughout the photocatalytic reaction to supply oxygen in addition to attain the required stirring. After certain intervals from the beginning of the Vis light illumination, specimens were withdrawn from the illuminated suspension. The nanorods photocatalyst were detached from the illuminated suspension via filtration. After that, UV-vis spectrophotometer was practiced to inspect the photocatalytic destruction performance ( $\lambda_{\max}$  of CIP = 277 nm). The photocatalytic performance (PP, %) was evaluated adopting the following equation:

$$\text{PP (\%)} = (C_0 - C) / C_0 \times 100$$

where  $C_0$  is the initial concentration of CIP and  $C$  is the remaining concentration of CIP after each time interval of illumination.

## Results and discussion

Phase architecture, microstructure, and morphology of the formulated nanorods photocatalysts

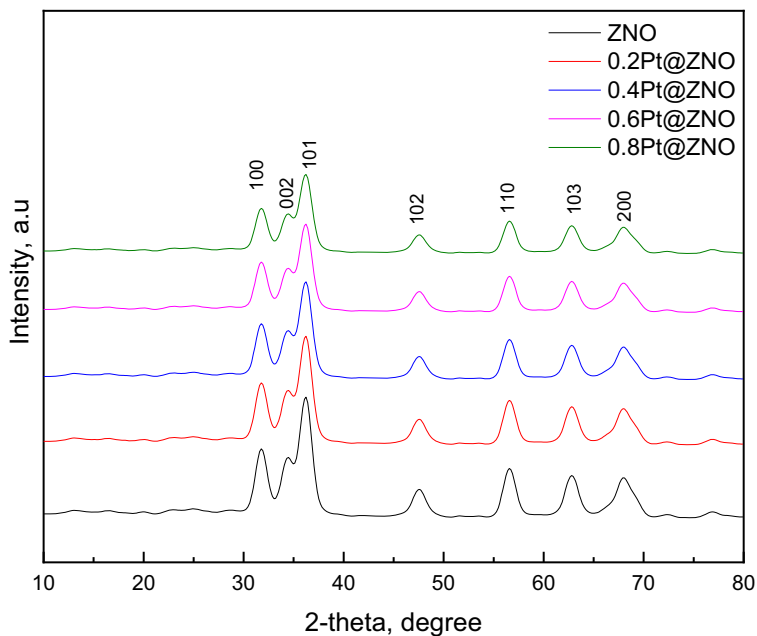
Figure 1 presents XRD diffractograms of the fabricated Pt@ZnO nanorods photocatalysts accommodating various proportions of Pt. Development of the ZnO phase within the various specimens was confirmed through the companionship of the peaks characterizing ZnO phase (JCPDS-89-0510). Furthermore, diffractograms of the doped nanorods photocatalysts emphasize that doping of mesoporous ZnO with Pt metal does not modify the crystalline phase of the fabricated ZnO. Nonetheless, doping ZnO nanorods photocatalyst with Pt is detected to shift the peak corresponding to (100) plane to a reduced angle. Although this finding affirms that Pt affects the position of the peak correlated to (100) plane, but at the same time, the detected shift is so small that impregnation of Pt into the ZnO matrix could not be confirmed. Table 1 exhibits the predicted crystallite size (D) adopting Scherrer relation in addition to the (100)

peak shift magnitudes of the diverse fabricated nanorods photocatalysts. It is obvious from the data of Table 1 that pure ZnO nanorods photocatalyst possesses a crystallite size of 5.0 nm, and this value is boosted to 7.0 and 6.0 nm upon doping ZnO nanorods photocatalysts with 0.6 and 0.8 wt.% Pt, respectively.

Figure 2 depicts the XPS measurements of the fabricated ZnO nanorods photocatalyst accommodating 0.6 wt.% Pt. Figure 2 presents two observable peaks at 1044.7 and 1021.6 eV that is characterized to Zn2p<sub>1/2</sub> and Zn2p<sub>3/2</sub>, respectively. This observation affirms the presence of Zn<sup>2+</sup> ions within the fabricated nanorods photocatalyst. Also, there is a distinct peak realized at 530.1 eV which could be correlated to O1s (Fig.2b). This observation endorses the presence of an oxide lattice phase within the fabricated nanorods photocatalyst. On the other hand, there are two distinct peaks at 71.0 eV and 74.4 eV that characterize Pt4f<sub>7/2</sub> and Pt4f<sub>5/2</sub>, respectively (Fig.2c). This inspection confirms the existence of Pt metal within the fabricated doped specimen.

Figure 3 presents HRTEM inspection of the various fabricated ZnO nanorods photocatalysts accommodating 0 and 0.6 wt.% Pt. Figure 3a clarifies the nanorods architecture of the fabricated mesoporous ZnO nanospecimen. On the other hand, the HRTEM image of the ZnO nanorods photocatalyst accommodating 0.6 wt.% Pt exhibits district dots with a particle size of 4.2–4.6 nm on the surface of the nanorods (Fig. 3b). The observed dots are correlated to Pt metal particles that are highly dispersed on the surface of ZnO nanorods. It is clear that the inclusion of Pt metal dopant to ZnO nanorods does not alter their architecture. Furthermore, Fig. 3c exhibits the lattice-resolution micrograph of the fabricated ZNO accommodating 0.6 wt.% Pt. Figure 3c depicts the appearance of dots on the surface of the nanorods confirming the dispersion of dopant metal atoms (Pt) as dots on ZnO nanorods. Development of the ZnO lattice arrangement is affirmed by the appearance of the lattice spacing of about 0.270 nm that characterizes the lattice spacing of the ZnO plane (002), whereas the development of the metallic Pt lattice arrangement is corroborated by distinguishing the lattice spacing of about 0.220 nm that characterizes the lattice spacing of the Pt plane (111).

Table 1 exhibits the surface characteristics of the fabricated ZnO nanorods photocatalysts accommodating diverse proportions of Pt. Table 1 illustrates that the specific surface area possessed by ZnO nanorods photocatalyst accommodating 0 wt.% Pt is 200 m<sup>2</sup>/g, whereas the

**Fig. 1** XRD patterns of ZNO and Pt@ZNO samples

specific surface area of the fabricated ZnO nanorods photocatalyst accommodating 0.8 wt.% Pt is 225 m<sup>2</sup>/g. The data of Table 1 clarifies that the inclusion of metallic Pt metal as dopant increases the specific surface areas of the various ZnO nanorods photocatalysts and the enlargement in the surface areas is boosted by increasing the Pt dopant percentage. Obviously, Table 1 depicts that the average pore volume of the fabricated nanorods photocatalysts increases with the enlargement of the Pt metal dopant proportions. The parallel correlation between average pore volume and specific surface area of the fabricated nanorods photocatalysts could be correlated to the pore widening of the various nanorods photocatalysts as the result of metallic Pt inclusion.

Figure 4 exhibits adsorption-desorption isotherm of the ZnO nanorods photocatalysts accommodating 0 and

0.6 wt. It is obvious from the data of Fig. 4 that undoped and doped nanorods photocatalysts possess isotherms of type IV. The displayed isotherms are characterized by adsorption of multilayer and subsequent capillary condensation. Furthermore, the mesoporous architecture of the investigated nanorods photocatalysts is affirmed by the appearance of hysteresis at higher relative pressure. The data of Fig. 4 clarifies also that the average pore diameter and the pore volume of the fabricated ZnO nanorods photocatalyst accommodating 0.8 wt.% Pt are 7.29 nm and 0.198 cm<sup>3</sup>g<sup>-1</sup>, respectively. Evidently, the surface area possessed by the fabricated mesoporous ZnO nanorods photocatalyst is 200 m<sup>2</sup>/g which is seven times greater than that of bulk ZnO; up to our knowledge, this large surface area wasn't attained previously. It could be concluded that some sort of pore widening, pore volume enlargement, and surface area growth might occur for the doped ZnO nanorods photocatalysts as the result of metallic Pt inclusion and the estimated gap increases by boosting of the Pt dopant proportions.

**Table 1** Textural properties of ZNO and Pt@ZNO samples

Sample	$S_{BET}$ (m <sup>2</sup> /g)	$V_p$ (cm <sup>3</sup> /g)	$D_p$ (nm)	$D$ (nm)
ZNO	200	0.140	6.90	5.0
0.2 Pt@ZNO	210	0.156	7.20	5.5
0.4 Pt@ZNO	215	0.170	7.25	6.2
0.6 Pt@ZNO	220	0.184	7.28	7.0
0.8 Pt@ZNO	225	0.198	7.29	6.0

$S_{BET}$  surface area,  $V_p$  pore volume,  $D_p$  pore diameter, and  $D$  Crystallite Size

#### Optical and optoelectronic properties of ZNO and Pt@ZNO nanorods photocatalysts

It is well known that the optical features of the fabricated nanocomposites affect greatly their photocatalytic performance. Absorption spectra of the fabricated ZnO nanorods photocatalysts accommodating diverse

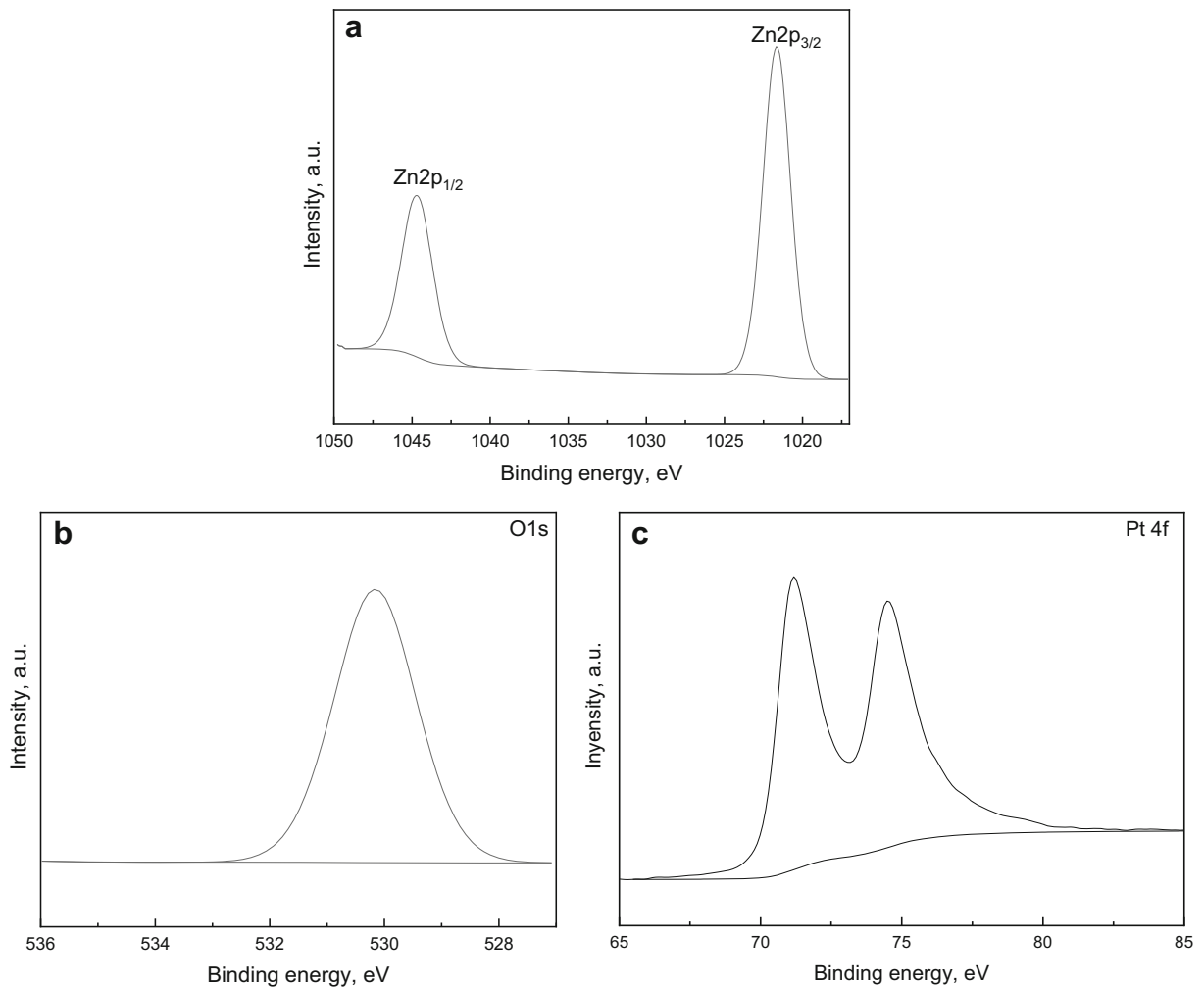


**Fig. 2** High-resolution XPS spectra of 0.6 Pt@ZNO sample, where **a** Zn2p, **b** O1s, and **c** Pt4f

proportions of metallic Pt are exhibited in Fig. 5. Figure 5 depicts that the fabricated mesoporous ZnO nanorods photocatalyst accommodating 0 wt.% Pt exhibits no absorption in the Vis zone. Nevertheless, the inclusion of metallic Pt as a dopant is found to displace the absorption toward Vis zone (the absorption edges are shifted to longer wavelengths). The registered absorption edges for the fabricated mesoporous ZNO nanorods photocatalysts accommodating 0, 0.2, 0.4, 0.6, and 0.8 wt.% Pt are 385, 440, 454, 475, and 476 nm, respectively. Obviously, the light absorption possessed by ZnO nanorods photocatalyst accommodating 0.6 wt.% Pt is nearly the greatest one amid other nanorods photocatalysts. Hence, the inclusion of Pt to ZnO nanorods photocatalysts boosts the light absorption toward the Vis zone. Table 2 exhibits the band gap energies ( $E_g$ )

of the diverse nanorods photocatalysts. It is clear from the data of Table 2 that the inclusion of 0.8 wt.% Pt to mesoporous ZnO nanorods diminishes the band gap energy from 3.20 to 2.62 eV.

The advancement of the optoelectronic features of the fabricated ZnO nanorods photocatalysts could be also inspected by the PL spectra acquired by these specimens. The transformation of the photo-generated e<sup>-</sup>s from conduction band (CB) to valence band (VB) could be reflected from the PL emission spectra. Figure 6 affirms that inclusion of metallic Pt, as dopant, to mesoporous ZnO nanorods photocatalysts enhances the PL peak magnitudes from 386 nm (possessed by pure ZnO nanorods photocatalyst) to greater emission wavelengths, and at the same time, the PL peak



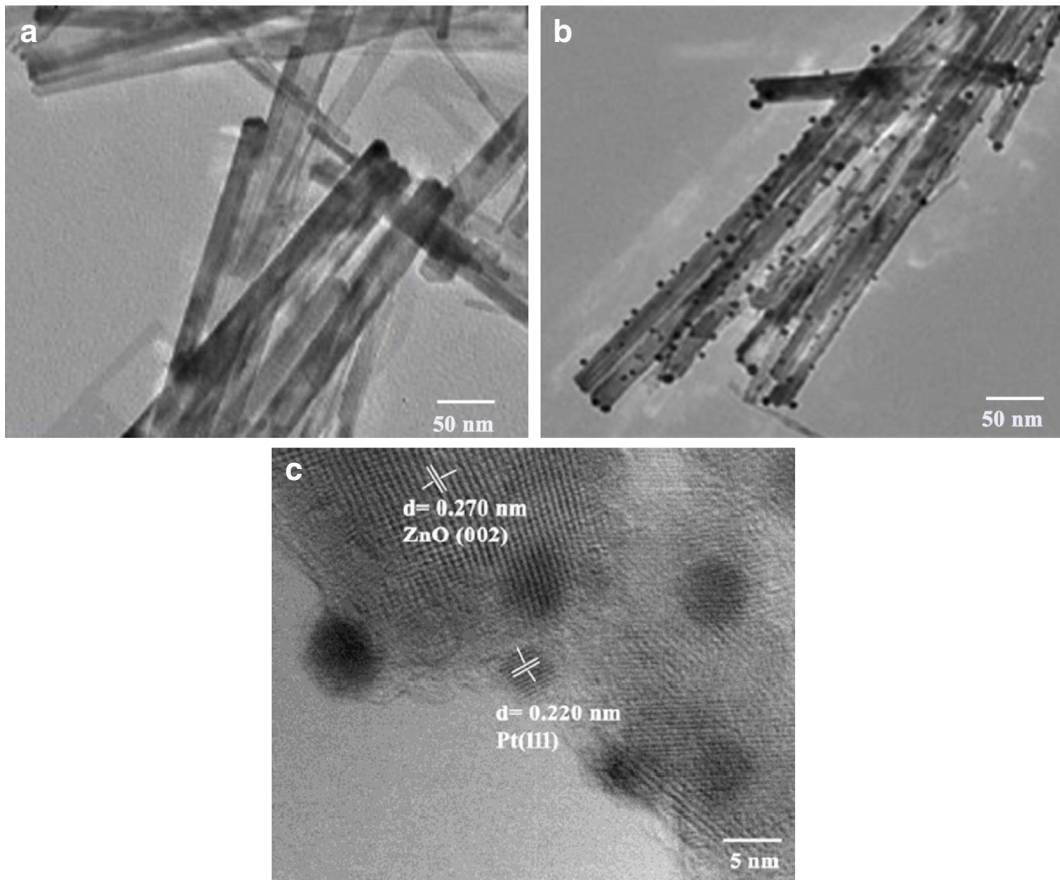


**Fig. 3** TEM images of ZnO(A) and 0.6 Pt@ZNO(B) and HRTEM image of 0.6 Pt@ZNO sample (C)

**Fig. 4** Adsorption -desorption isotherm of ZnO and 0.6 Pt@ZNO photocatalysts

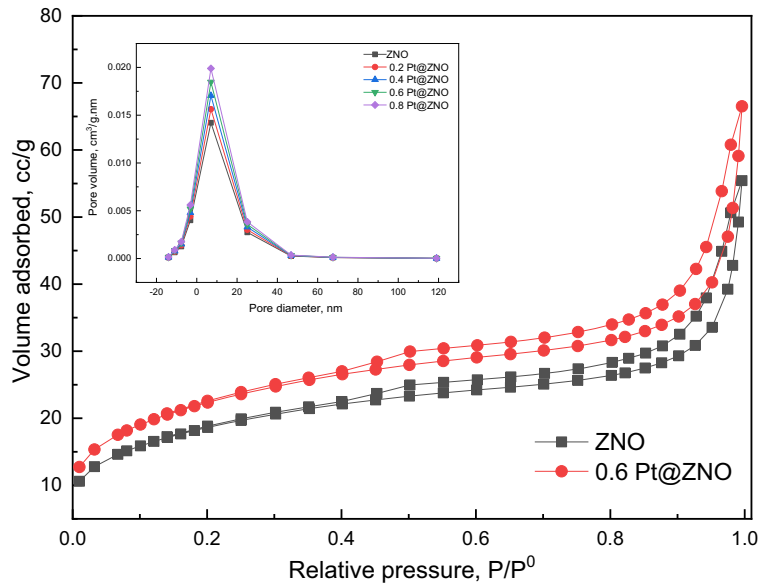
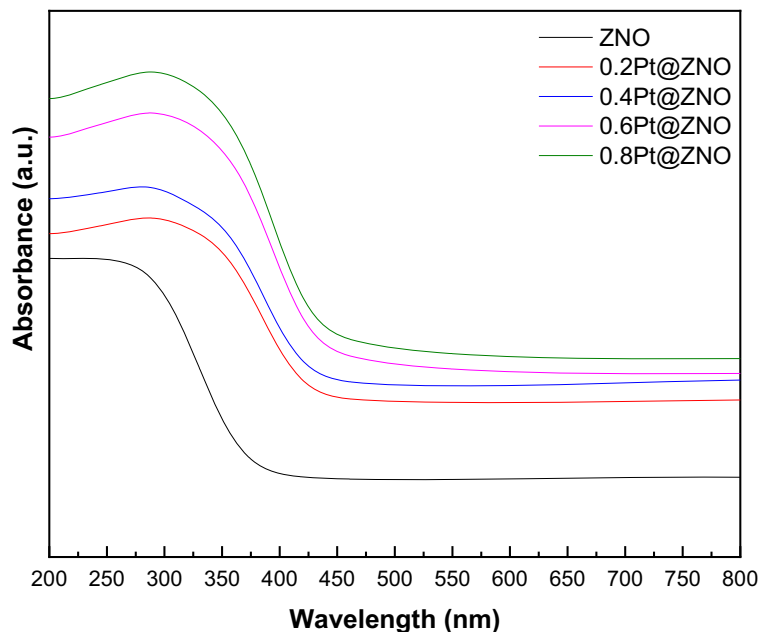


**Fig. 5** UV-Vis spectra of ZNO and Pt@ZNO samples



magnitudes are boosted by increasing the metallic Pt proportions. This observation demonstrates that a mid-gap levels generated by metallic Pt inclusion were diminished to reduced energy states. Furthermore, Fig. 6 clarifies that the mesoporous ZnO nanorods photocatalyst accommodating 0.6 wt.% Pt possesses nearly the minimum PL peak intensity (comparable with that of 0.8 Pt@ZnO nanorods photocatalyst) emerged at 475 nm. It could be concluded that inclusion of metallic Pt to ZnO nanorods photocatalyst retards the electron-hole recombination that attains nearly its minimal speed by the inclusion of 0.6 wt.% Pt. Evidently, although the PL peak intensity attained by 0.8 Pt@ZnO photocatalyst is the minimum, but due to the economic reasons, we considered 0.6 Pt@ZnO photocatalyst as the preferable composition; especially, it possesses comparable value with

that of 0.8 Pt@ZnO photocatalyst. In conclusion, incorporation of metallic Pt to ZnO nanorods photocatalyst suppresses the electron-hole recombination speed through acting as a sink for the photo-generated electrons that by its role, enhances the photocatalytic performance.

#### Photocatalytic remediation of CIP using ZNO and Pt@ZNO photocatalysts

##### *Impact of doping with Pt*

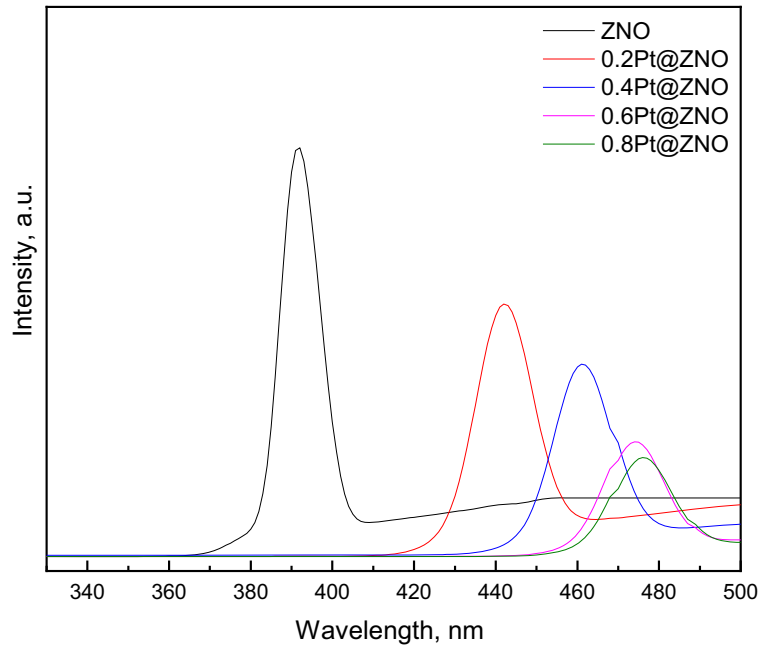
Photocatalytic destruction percentage of CIP vs time of Vis light irradiation adopting the diverse fabricated ZnO nanorods photocatalysts is exhibited in Fig. 7. It is noticed from the data of Fig. 7 that the photocatalytic destruction percentage of CIP is boosted with the time of illumination for all investigated nanorods photocatalysts. Each specimen was utilized with a dose of 0.8 g/L. It is obvious from the data of Fig. 7 that the photocatalytic destruction percentage of CIP over the mesoporous ZnO nanorods photocatalyst accommodating 0 wt.% Pt is very small (10%), whereas the percentages of the photocatalytic destruction of CIP over ZnO nanorods photocatalysts accommodating 0.2, 0.4, 0.6, and 0.8 wt.% Pt are estimated to be 44, 75, 100, and 100%, respectively, after 120 min of

**Table 2** Band gap energy of ZnO and Pt@ZnO samples

Sample	Band gap (eV)
ZNO	3.22
0.2 Pt@ZNO	2.82
0.4 Pt@ZNO	2.73
0.6 Pt@ZNO	2.63
0.8 Pt@ZNO	2.62



**Fig. 6** PL spectra of ZnO and Pt@ZNO samples



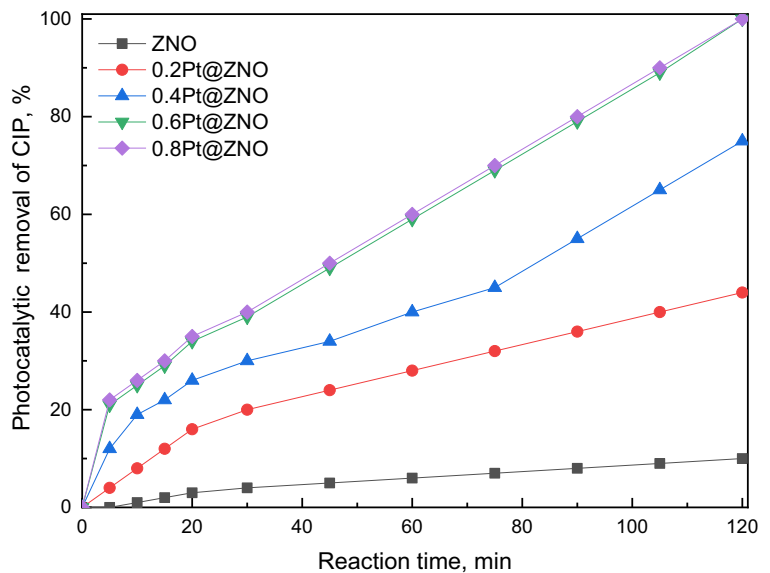
illumination. Hence, the inclusion of metallic Pt to ZnO nanorods photocatalysts enhances their photocatalytic performance toward CIP remediation. Evidently, mesoporous ZnO nanorods photocatalyst accommodating 0.6 wt.% could photo-degrade CIP completely after 120 min of Vis light illumination. The enhanced photocatalytic performance of the fabricated ZnO nanorods photocatalysts accommodating diverse proportions of metallic Pt could be

correlated to the depressed recombination amid the photo-generated carriers, improved surface characteristics, and boosted light absorption.

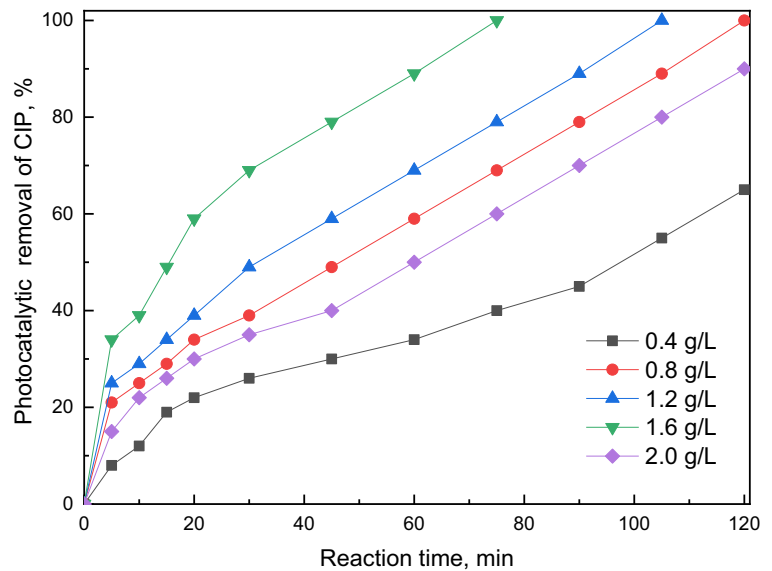
*Impact of 0.6 Pt@ZNO doses on photocatalytic performance and recyclability*

Figure 8 demonstrates the consequence of the dose of Pt@ZNO accommodating 0.6 wt.% Pt, as an optimum

**Fig. 7** Effect of Pt doping on the degradation of CIP



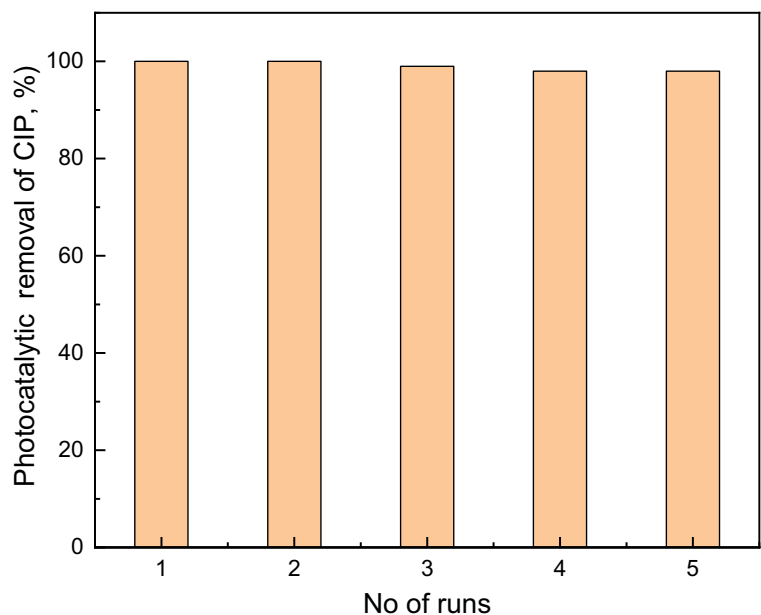
**Fig. 8** Effect of dose of 0.6 Pt@ZNO photocatalysts on the degradation of CIP



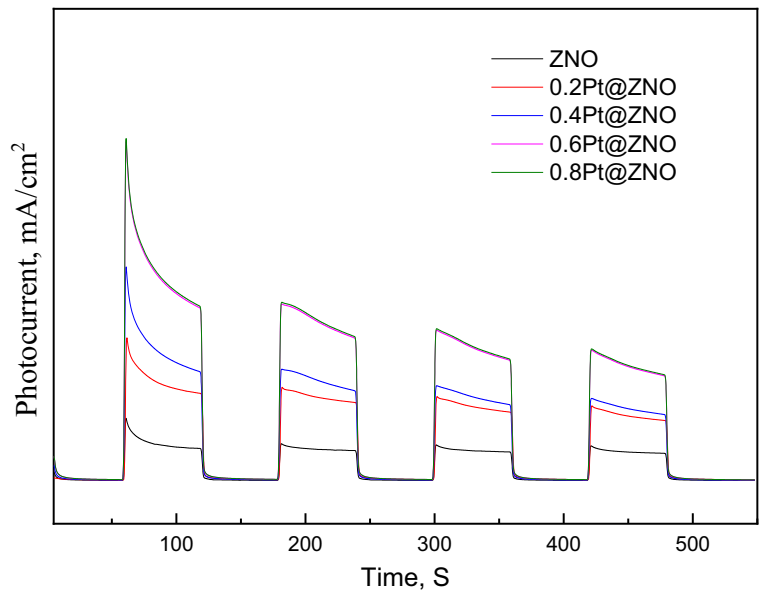
construction, toward CIP destruction. This investigation was performed utilizing 0.6 Pt@ZNO photocatalyst dose between 0.4 to 2.0 gL<sup>-1</sup>. The data of Fig. 8 demonstrates that photo-destruction of CIP is enhanced continuously up on boosting 0.6 Pt@ZNO photocatalyst dose to 1.6 gL<sup>-1</sup>. Evidently, photocatalytic destruction of CIP is completed (100%) after 75 min of Vis light illumination upon application of 1.6 gL<sup>-1</sup> of 0.6 Pt@ZNO photocatalyst, whereas up on the application of 0.4, 0.8, and 1.2 gL<sup>-1</sup> of 0.6

Pt@ZNO photocatalyst, the photocatalytic destruction of CIP reaches 65, 100, and 100% after 120, 120, and 105 min of Vis light illumination, respectively. This observation might be correlated to the boosted number of active sites available to the photocatalytic reaction. Contrarily, adopting 2.0 gL<sup>-1</sup> of 0.6 Pt@ZNO photocatalyst diminishes the photocatalytic performance toward CIP degradation to 90% after 120 min of Vis light illumination. The reduced performance up on adopting a large dose of

**Fig. 9** Effect of recycling of 0.6 Pt@ZNO photocatalysts on the degradation of CIP



**Fig. 10** Photocurrent transient response of ZNO and Pt@ZNO samples



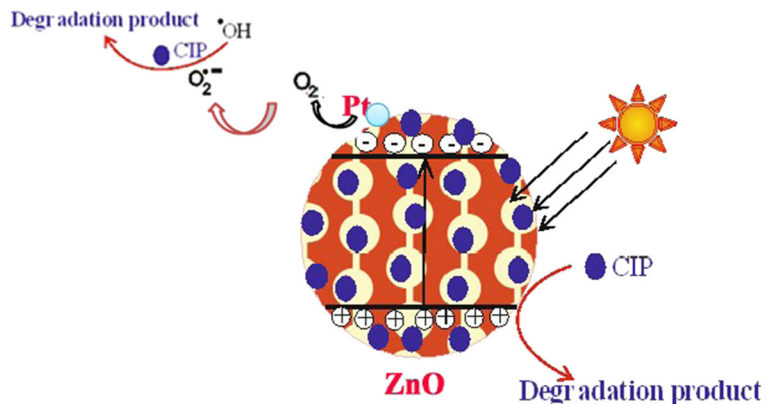
0.6 Pt@ZNO photocatalyst is ascribed to the accumulation of the photocatalyst molecules that serve as a boundary to the passage of the Vis light to photocatalyst surface. Accordingly, the number of accessible active centers is diminished which brings about reduced photocatalytic performance.

Figure 9 exhibits the recycling experiment of the utilized Pt@ZNO photocatalyst accommodating 0.6 wt.% metallic Pt. The attained measurements of Fig. 9 indicate great performance and excellent recyclability of the applied photocatalyst after application many cycles. Evidently, the photocatalytic efficiency of the applied photocatalyst could preserve about 98% of its reachable magnitude after the 5th cycle. Hence, mesoporous Pt@ZnO

photocatalyst accommodating 0.6 wt.% metallic Pt exhibits pronounced reusability and could be applied as beneficial, economical, and commercial photocatalyst for pollutant removal.

Figure 10 demonstrates the photocurrent transient response of the mesoporous ZnO photocatalysts accommodating diverse proportions of metallic Pt. The photocurrent response for the pure mesoporous ZnO nanorods photocatalyst and ZnO nanorods photocatalyst accommodating 0.6 wt.% Pt is recorded at 0.0044 and 0.023 mA cm<sup>-2</sup>, respectively. The boosting of the photocurrent transient response as a result of metallic Pt inclusion could be ascribed to the improvement of charge separation in addition to the enhancement of the electrical features.

**Fig. 11** The photocatalytic mechanism of CIP oxidation by using the Pt@ZNO photocatalyst



### Mechanism of the photocatalytic action

Figure 11 exhibits the mechanism of the photocatalytic destruction of CIP adopting Pt@ZnO photocatalysts accommodating metallic Pt. Evidently, electrons and holes are being photo-generated after Vis light illumination that is contributed to the photocatalytic action. The photo-generated e<sup>-</sup>s in the conduction band (CB) of ZnO can be readily transported to metallic Pt, which functions as a sink of e<sup>-</sup>s. Accordingly, the rate of electron-hole recombination is undoubtedly diminished. Then, the generated charges react with adsorbed water molecules and oxygen molecules to produce oxidized species. Hence, CIP could be oxidized and degraded via the generated hydroxyl radicals and oxygen molecules to develop water and carbon dioxide molecules. The importance of Pt inclusion is concerned in developing intermediate-level beneath the CB of the ZnO in which electrons and holes are being readily transferred. Furthermore, the diminished E<sub>g</sub> and the enhanced surface features contribute strongly to the improvement of the performance of the Pt@ZnO photocatalysts.

### Conclusion

The following outcomes could be driven based on our investigation:

- 1- Mesoporous ZNO photocatalysts accommodating diverse proportions of metallic Pt were successfully fabricated via a facile one-pot regime.
- 2- The surface area possessed by the fabricated mesoporous ZnO nanorods photocatalysts was 200 m<sup>2</sup>/g.
- 3- Inclusion of metallic Pt to ZNO nanorods photocatalysts enhanced both surface features in addition to the photocatalytic performance of the doped ZNO photocatalysts.
- 4- Photocatalytic performance of the fabricated nanorods photocatalysts was tested via the degradation of CIP as a model.
- 5- Complete photocatalytic destruction of CIP was accomplished after 75 min of Vis light illumination adopting 1.6 gL<sup>-1</sup> mesoporous ZNO nanorods photocatalyst accommodating 0.6 wt.% metallic Pt.
- 6- The pronounced photocatalytic performance of the doped ZNO photocatalysts is ascribed to the suppressed electron-hole recombination, diminished

band gap magnitudes, enlarged Vis light absorption, and improved surface features.

- 7- 0.6 Pt@ZNO photocatalyst exhibited great stability accompanied by pronounced recyclability after reusing five cycles.
- 8- This investigation provides an application of ZNO photocatalysts for remediation of CIP from wastewater adopting Vis light illumination.

### Compliance with ethical standards

**Conflict of interest** The authors declare that they have no conflict of interest.

### References

- Abdennouri M, Elhalil A, Farnane M, Tounsadi H, Mahjoubi FZ, Elmoubarki R, Sadiq M, Khamar L, Galadi A, Baâlala M, Bensitel M, El Hafiane Y, Smith A, Barka N (2015) Photocatalytic degradation of 2,4-D and 2,4-DP herbicides on Pt/TiO<sub>2</sub> nanoparticles. *J Saudi Chem Soc* 19:485–493
- Akhundi A, Habibi-Yangjeh A, Abitorabi M, Rahim Pourn S (2019) Review on photocatalytic conversion of carbon dioxide to value-added compounds and renewable fuels by graphitic carbon nitride-based photocatalysts. *Catal Rev* 61(4): 595–628
- An T, Yang H, Li G, Song W, Cooper WJ, Nie X (2010) Kinetics and mechanism of advanced oxidation processes (AOPs) in degradation of ciprofloxacin in water. *Appl Catal B* 94:288–294
- Antonin VS, Santos MC, Garcia-Segura S, Brillas E (2015) Electrochemical incineration of the antibiotic ciprofloxacin in sulfate medium and synthetic urine matrix. *Water Res* 83: 31–41
- Baoum AA, Amin MS, Mohamed RM (2018) Decoration of SnO<sub>2</sub> nanosheets by AgI nanoparticles driven visible light for norfloxacin degradation. *Appl Nanosci* 8:2093–2102
- Baoum A, Amin MS, Mohamed RM (2020) Development of CuCr<sub>2</sub>O<sub>4</sub> nanocomposite adopting decoration with polyaniline for acridine orange dye degradation. *Appl Nanosci* 10:1501–1510
- Bolong N, Ismail AF, Salim MR, Matsuura T (2009) A review of the effects of emerging contaminants in wastewater and options for their removal. *Desalination* 239:229–246
- Bonakdarpour B, Vyrides I, Stuckey DC (2011) Comparison of the performance of one stage and two stage sequential anaerobic-aerobic biological processes for the treatment of reactive-azo-dye-containing synthetic wastewaters. *Int Biodeterior Biodegrad* 65:591–599
- Bousslama W, Elhouichet H, Férid M (2017) Enhanced photocatalytic activity of Fe doped ZnO nanocrystals under sunlight irradiation. *Optik* 134:88–98

- Cai A, Guo A, Du L, Qi Y, Wang X (2018) Leaf-templated synthesis of hierarchical AgCl-Ag-ZnO composites with enhanced visible-light photocatalytic activity. *Mater Res Bull* 103:225–233
- Chakraborty S, Loutatidou S, Palmisano G, Kujawa J, Mavukkandy MO, Al-Gharabli S, Curcio E, Arafat HA (2017) Photocatalytic hollow fiber membranes for the degradation of pharmaceutical compounds in wastewater. *J Environ Chem Eng* 5:5014–5024
- Daneshvar N, Salari D, Khataee AR (2004) Photocatalytic degradation of azo dye acid red 14 in water on ZnO as an alternative catalyst to TiO<sub>2</sub>. *J Photochem Photobiol A Chem* 162: 317–322
- Daughton CG, Ternes TA (1999) Pharmaceuticals and personal care products in the environment: agents of subtle change? *Environ Health Perspect* 107:907–938
- Djurišić AB, Leung YH (2006) Optical properties of ZnO nanostructures. *Small* 2:944–961
- Elhalil A, Tounsadi H, Elmoubarki R, Mahjoubi FZ, Farnane M, Sadiq M, Abdennouri M, Qourzal S, Barka N (2016) Factorial experimental design for the optimization of catalytic degradation of malachite green dye in aqueous solution by Fenton process. *Water Resour Ind* 15:41–48
- Freitas TKFS, Oliveira VM, de Souza MTF, Geraldino HCL, Almeida VC, Fávoro SL, Garcia JC (2015) Optimization of coagulation-flocculation process for treatment of industrial textile wastewater using okra (*A. esculentus*) mucilage as natural coagulant. *Ind Crops Prod* 76:538–544
- Georgekutty R, Seery MK, Pillai SC (2008) A highly efficient Ag-ZnO photocatalyst: synthesis, properties, and mechanism. *J Phys Chem C* 112:13563–13570
- Hariharan C (2006) Photocatalytic degradation of organic contaminants in water by ZnO nanoparticles: revisited. *Appl Catal A Gen* 304:55–61
- Ismail AA, Mohamed RM, Fouad OA, Ibrahim IA (2006) Synthesis of nanosized ZSM-5 using different alumina sources. *Cryst Res Technol* 41(2):145–149
- Jaramillo-Páez C, Navío JA, Hidalgo MC (2018) Silver-modified ZnO highly UV-photoactive. *J Photochem Photobiol A Chem* 356:112–122
- Jodat A, Jodat A (2014) Photocatalytic degradation of chloramphenicol and tartrazine using Ag/TiO<sub>2</sub> nanoparticles. *Desalin Water Treat* 52:2668–2267
- Kansal SK, Singh M, Sud D (2007) Studies on photodegradation of two commercial dyes in aqueous phase using different photocatalysts. *J Hazard Mater* 141:581–590
- Kochuveedu ST, Jang YH, Kim DH (2013) A study on the mechanism for the interaction of light with noble metal-metal oxide semiconductor nanostructures for various photophysical applications. *Chem Soc Rev* 42:8467–8493
- Li X, Liu H, Cheng L, Tong H (2003) Photocatalytic oxidation using a new catalyst TiO<sub>2</sub> microsphere for water and wastewater treatment. *Environ Sci Technol* 37:3989–3994
- Lin D, Wu H, Zhang R, Pan W (2009) Enhanced Photocatalysis of electrospun Ag-ZnO heterostructured nanofibers. *Chem Mater* 21:3479–3484
- Liqiang J, Dejun W, Baiqi W, Shudan L, Baifu X, Honggang F, Jiazhong S (2006) Effects of noble metal modification on surface oxygen composition, charge separation and photocatalytic activity of ZnO nanoparticles. *J Mol Catal A Chem* 244:193–200
- Liu Y, Xu C, Zhu Z, Lu J, Manohari AG, Shi Z (2018) Self-assembled ZnO/Ag hollow spheres for effective photocatalysis and bacteriostasis. *Mater Res Bull* 98:64–69
- Ma S, Xue J, Zhou Y, Zhang Z (2014) Photochemical synthesis of ZnO/Ag<sub>2</sub>O heterostructures with enhanced ultraviolet and visible photocatalytic activity. *J Mater Chem A* 2:7272–7280
- Mahjoubi FZ, Khalidi A, Abdennouri M, Barka N (2016) M-Al-SO<sub>4</sub> layered double hydroxides (M=Zn, Mg or Ni): synthesis, characterization and textile dyes removal efficiency. *Desalin Water Treat* 57:21564–21576
- Miyauchi M, Nakajima A, Watanabe T, Hashimoto K (2002) Photocatalysis and photoinduced hydrophilicity of various metal oxide thin films. *Chem Mater* 14:2812–2816
- Mohamed RM (2009) Characterization and catalytic properties of nano-sized Pt metal catalyst on TiO<sub>2</sub>-SiO<sub>2</sub> synthesized by photo-assisted deposition and impregnation methods. *J Mater Process Technol* 209(1):577–583
- Mohamed RM, Aazam E (2013) Synthesis and characterization of P-doped TiO<sub>2</sub> thin-films for photocatalytic degradation of butyl benzyl phthalate under visible-light irradiation. *Chin J Catal* 34(6):1267–1273
- Mohamed RM, Salam MA (2014) Photocatalytic reduction of aqueous mercury (II) using multi-walled carbon nanotubes/Pd-ZnO nanocomposite. *Mater Res Bull* 50:85–90
- Mohamed RM, Mkhallid IA, Baeissa ES, Al-Rayyani MA (2012) Photocatalytic degradation of methylene blue by Fe/ZnO/SiO<sub>2</sub> nanoparticles under visible light. *J Nanotechnol* 2012: 1–5
- Mohamed RM, Shawky A, Mkhallid IA (2017) Facile synthesis of MgO and Ni-MgO nanostructures with enhanced adsorption of methyl blue dye. *J Phys Chem Solids* 101:50–57
- Mu J, Shao C, Guo Z, Zhang Z, Zhang M, Zhang P, Chen B, Liu Y (2011) High photocatalytic activity of ZnO-carbon nanofiber heteroarchitectures. *ACS Appl Mater Interfaces* 3:590–596
- Pirhashemi M, Habibi-Yangjeh A, Pouran SR (2018) Review on the criteria anticipated for the fabrication of highly efficient ZnO-based visible-light-driven photocatalysts. *J Ind Eng Chem* 62:1–25
- Plodinec M, Gajović A, Jakša G, Žagar K, Čeh M (2014) High-temperature hydrogenation of pure and silver-decorated titanate nanotubes to increase their solar absorbance for photocatalytic applications. *J Alloys Compd* 591:147–155
- Qiu X, Li L, Zheng J, Liu J, Sun X, Li G (2008) Origin of the enhanced photocatalytic activities of semiconductors: a case study of ZnO doped with Mg<sup>2+</sup>. *J Phys Chem C* 112:12242–12248
- Ravelli D, Dondi D, Fagnoni M, Albini A (2009) Photocatalysis. A multi-faceted concept for green chemistry. *Chem Soc Rev* 38:1999–2011
- Sacco O, Vaiano V, Matarangolo M (2018) ZnO supported on zeolite pellets as efficient catalytic system for the removal of caffeine by adsorption and photocatalysis. *Sep Purif Technol* 193:303–310
- Sardar D, Maity J, Ghosal MK, Gopinath CS, Bala T (2017) Facile synthesis of ZnO-Ag nanocomposite and its photocatalytic activity. *Mater Res Express* 4:055011
- Sarkar S, Makhil A, Bora T, Baruah S, Dutta J, Pal SK (2011) Photosensitive excited state dynamics in ZnO-Au nanocomposites and their implications in photocatalysis and dye-sensitized solar cells. *Phys Chem Chem Phys* 13:12488–12496

- Shekofteh-Gohari M, Habibi-Yangjeh A, Abitorabi M, Rouhi A (2018) Magnetically separable nanocomposites based on ZnO and their applications in photocatalytic processes: a review. *Crit Rev Environ Sci Technol* 48(10–12):806–857
- Sobahi TR, Amin MS (2020) Synthesis of ZnO/ZnFe<sub>2</sub>O<sub>4</sub>/ Pt nanoparticles heterojunction photocatalysts with superior photocatalytic activity. *Ceram Int* 46:3558–3564
- Sobahi TR, Amin MS, Mohamed RM (2018) Enlargement of photocatalytic efficiency of BaSnO<sub>3</sub> by indium doping for thiophene degradation. *Appl Nanosci* 8:557–565
- Sohabi T, Amin MS, Mohamed RM (2017) Photocatalytic degradation of methylene blue dye by F-doped Co<sub>3</sub>O<sub>4</sub> nanowires. *Desalin Water Treat* 74:346–353
- Sudrajat H, Babel S (2017) A novel visible light active N-doped ZnO for photocatalytic degradation of dyes. *J Water Process Eng* 16:309–318
- Suryavanshi RD, Mohite SV, Bagade AA, Shaikh SK, Thorat JB, Rajpure KY (2018) Nanocrystalline immobilised ZnO photocatalyst for degradation of benzoic acid and methyl blue dye. *Mater Res Bull* 101:324–333
- Taheran M, Brar SK, Verma M, Surampalli RY, Zhang TC, Valero JR (2016) Membrane processes for removal of pharmaceutically active compounds (PhACs) from water and wastewaters. *Sci Total Environ* 547:60–77
- Tanaka A, Kominami H (2016) Plasmonic photocatalysts: preparation and evaluation. In: Yamashita H, Li H (eds) *Nanostructured photocatalysts: advanced functional materials*. Springer International Publishing, Cham, pp 281–292
- Truong NNK, Trung TN, Tu N, Nghia NV, Thuy DM (2013) Preparation and characterisation of silver doped ZnO nanostructures. *Int J Nanotechnol* 10:260–268
- Ullah R, Dutta J (2008) Photocatalytic degradation of organic dyes with manganese-doped ZnO nanoparticles. *J Hazard Mater* 156:194–200
- Vaiano V, Matarangolo M, Sacco O, Sannino D (2017) Photocatalytic treatment of aqueous solutions at high dye concentration using praseodymium-doped ZnO catalysts. *Appl Catal B Environ* 209:621–630
- Vaiano V, Matarangolo M, Murcia JJ, Rojas H, Navío JA, Hidalgo MC (2018) Enhanced photocatalytic removal of phenol from aqueous solutions using ZnO modified with Ag. *Appl Catal B Environ* 225:197–206
- Vijayan BL, Misnon II, Kumar GMA, Miyajima K, Reddy MV, Zaghbi K et al (2020) Facile fabrication of thin metal oxide films on porous carbon for high density charge storage. *J Colloid Interface Sci* 562:567–577
- Wang CM, Heller A, Gerischer H (1992) Palladium catalysis of O<sub>2</sub> reduction by electrons accumulated on TiO<sub>2</sub> particles during photoassisted oxidation of organic compounds. *J Am Chem Soc* 114:5230–5234
- Wang P, Huang B, Dai Y, Whangbo MH (2012) Plasmonic photocatalysts: harvesting visible light with noble metal nanoparticles. *Phys Chem Chem Phys* 14:9813–9825
- Wang F, Zhao D, Xu Z, Zheng Z, Zhang L, Shen D (2013) Monochromatic visible light-driven photocatalysis realized on 2D ZnO shell arrays. *J Mater Chem A* 1:9132–9137
- Wang L, Hou X, Li F, He G, Li L (2015) Hybrid ZnO/Ag nanocomposites: fabrication, characterization, and their visible-light photocatalytic activity. *Mater Lett* 161:368–371
- Wang H, Liu X, Han S (2016) The synthesis of a Ag–ZnO nanohybrid with plasmonic photocatalytic activity under visible-light irradiation: the relationship between tunable optical absorption, defect chemistry and photocatalytic activity. *Cryst Eng Commun* 18:1933–1943
- Yu ZB, Xie YP, Liu G, Lu GQ, Ma XL, Cheng HM (2013) Self-assembled CdS/au/ZnO heterostructure induced by surface polar charges for efficient photocatalytic hydrogen evolution. *J Mater Chem A* 1:2773–2776
- Yuan XZ, Wang H, Wu Y, Zeng GM, Chen XH, Leng LJ, Wu ZB, Li H (2016) One-pot self-assembly and photoreduction synthesis of silver nanoparticle-decorated reduced graphene oxide/MIL-125(Ti) photocatalyst with improved visible light photocatalytic activity. *Appl Organomet Chem* 30:289–296
- Zhang Y, Xu J, Wang Q, Pan Z, Ma S, Chen Q (2016) Preparation and properties of ZnO loaded with uniform Ag nanoparticles. *Mater Res Bull* 73:119–124

**Publisher's note** Springer Nature remains neutral with regard to jurisdictional claims in published maps and institutional affiliations.